ChemPlusChem

A Multidisciplinary Journal Centering on Chemistry

Chemistry Europe

European Chemical Societies Publishing

Accepted Article

Title: Carbidopa and ZnCarbidopa Induce Reductive Stress in MDA-MB-231 Cells

Authors: Agustin B. Actis Dato, Luciana G. Naso, Valeria R. Martínez, Evelina G. Ferrer, and Patricia Williams

To be cited as: *ChemPlusChem* **2024**, e202400596

Link to VoR: https://doi.org/10.1002/cplu.202400596

WILEY VCH

10.1002/cplu.202400596

Carbidopa and ZnCarbidopa Induce Reductive Stress in MDA-MB-231 Cells

Agustin B. Actis Dato,[a] Luciana G. Naso,*[a] Valeria R. Martínez,[b] Evelina G. Ferrer,[a] Patricia A.M. Williams*[a]

[a] Centro de Química Inorgánica (CEQUINOR-CONICET-UNLP- Asoc CICPBA)-Departamento de Química-Facultad de Ciencias Exactas, Universidad Nacional de La Plata, Boulevard 120 entre 60 y 64, C.C.962- (B1900AVV) -1900 La Plata, Argentina.
[b] CIC-CONICET-UNLP, Facultad de Médicas, Universidad Nacional de La Plata, 60 y 120, 1900 La Plata, Argentina

*To whom correspondence should be addressed
e-mails: Luciana Naso, lucianaaso504@hotmail.com
Patricia A. M. Williams, williams@quimica.unlp.edu.ar

ORCID
Agustín B. Actis Dato: 0000-0003-2678-2808
Luciana G. Naso: 0000-0003-4881-7450
Valeria R. Martínez: 0000-0003-3251-6979
Evelina G. Ferrer: 0000-0002-6343-5170
Patricia A.M. Williams: 0000-0002-1549-5873

Abstract
The redox imbalance, caused by depletion or generation of reactive oxygen species (ROS), is a key mechanism by which metal complexes exert anticancer effects. Carbidopa has shown the ability to inhibit the MDA-MB-231 cell line, a highly aggressive triple-negative human breast adenocarcinoma, by inducing reductive stress. The metal complex of carbidopa with zinc (ZnCarbi) was designed to modify carbidopa's structure and exhibited increased cytotoxicity against MDA-MB-231 cells. Interestingly, ZnCarbi selectively targets certain cancer cells, showing no impact on the viability of normal HEK293 (human embryonic kidney) cells or other cancer cell lines like A549 (human lung adenocarcinoma), LM3 (murine breast adenocarcinoma), or HCT116 (human colon cancer). Treatment with carbidopa and ZnCarbi induces reductive stress, decreases ROS levels, increases the GSH/GSSG ratio, and protects cells from H_2O_2-induced death. Both compounds also cause mitochondrial damage, leading to cell death, and exhibit antimetastatic effects by inhibiting cell migration and invasion of MDA-MB-231 cells. Interaction studies with bovine serum albumin showed moderate binding through hydrophobic association. Overall, ZnCarbi demonstrates enhanced anticancer properties compared to carbidopa alone, highlighting its potential as an anticancer and antimetastatic compound.

Keywords: cancer; carbidopa; reductive stress; metastasis; Zn carbidopa complex

Introduction

Breast cancer is a global health concern, affecting over two million women in 2022 and leading to 670,000 diagnoses.[1] The MDA-MB-231 breast cancer cell line is characterized as triple negative with absence of overexpression of human epidermal growth factor receptor 2 (HER2) and lack of estrogen receptor (ER), as well as progesterone receptor (PR). This type of cancer is highly aggressive, prompting the development of various treatment strategies, including chemotherapy, immunotherapy, and antibody-drug conjugates.[2,3]

Carbidopa, (2S)-3-(3,4-dihydroxyphenyl)-2-hydrazinyl-2-methylpropanoic acid, is an anti-Parkinson's medication used in symptomatic treatments. It is co-administered with L-dopa to prevent dopa-decarboxylase conversion of levodopa to dopamine (a crucial neurotransmitter) before crossing the blood-brain barrier (BBB). This mechanism ensures that L-dopa can cross the BBB and be converted into dopamine within the brain.[4] Furthermore, due to its structural similarity to phenylhydrazine, carbidopa can function as an agonist for the nuclear receptor AhR (aryl hydrocarbon receptor). It exhibits selective cytotoxicity against cancer cell lines. Activation of AhR has been observed to induce tumor suppression in breast, colon, and pancreatic cancers.[5] Carbidopa is effective in inhibiting the growth and proliferation of AR-positive LNCaP and MCF-7 prostate and breast cancer cell lines, respectively, but does not affect AR-independent DU145 and PC3 prostate cancer cells.[6,7] *In vitro* studies have shown that carbidopa inhibits tumor growth by promoting the degradation of the estrogen receptor (ER) in ERα-positive MCF-7 cell line. Its anticancer effect is less pronounced in ER-negative MDA-MB-231 cells. *In vivo,* carbidopa suppressed the growth of ER-positive breast cancer cells in mouse xenograft models.[8-10]

The zinc cation (Zn(II)) does not undergo redox reactions due to its filled d shell, and it is not considered a classical antioxidant, as it does not directly interact with ROS.[11] However, zinc acts as an antioxidant by targeting zinc-associated proteins. Zinc can inhibit the Nuclear factor κB (NF-κB) activation induced by lipopolysaccharide (LPS), ROS, or tumor necrosis factor α (TNF-α), reducing inflammatory cytokine expression and oxidative stress in cell culture models.[12] It regulates the gene expression of MTs, and supplementation has been shown to reduce tissue copper and iron levels, while increasing metallothioneins (MTs) and antioxidant enzymes. This suggests that zinc-induced MT synthesis helps decrease free radicals produced by copper and iron.[13] Additionally, zinc plays a dual role in the antioxidant enzyme copper/zinc superoxide dismutase (Cu/Zn SOD, SOD1), supporting both its structural stability and function, stabilizing the native structure and facilitating rapid copper cycling between Cu(I) and Cu(II) to remove superoxide radicals.[14] It also regulates NADPH oxidase (NOX) enzymes, which generate ROS; zinc deficiency increases the expression and activity of these enzymes, a condition that can be alleviated by zinc supplementation.[15] Both SOD1 and NADPH oxidase are necessary for glutathione redox systems.[16] Additionally, zinc can bind to negatively charged phospholipids in the cell membrane, protecting them from peroxidative damage.[17,11] Zinc modulates the expression of antioxidant enzymes through transcription factors like Nuclear factor erythroid 2-related factor 2 (Nrf2), which activates genes involved in antioxidant defense, including glutamate-cysteine ligase, essential for glutathione (GSH) synthesis.[18-20] Furthermore, zinc interacts with thiol groups in GSH, making the Zn/GSH complex less susceptible to oxidation and enhancing the cell's ability to counteract redox changes.[21,22] It has been reported that the cytotoxic mechanism of zinc oxide nanoparticles occurs by reductive stress, with the aforementioned cellular components playing crucial roles.[23] Thus, through these combined actions, zinc maintains oxidative balance and induces cells to a state of reductive stress. The biometal is involved in immune responses, apoptosis and activities related to antioxidant and anti-inflammatory functions. Zn deficiency has been linked to several diseases, including diabetes mellitus, depression and Alzheimer's disease.[24] cancer and cardiovascular conditions. Numerous meta-analyses have reported low Zn levels in hair and blood samples from individuals with breast cancer.[25] As a strong Lewis acid, Zn can interact with Lewis bases to form compounds with different coordination numbers. Zn complexes have shown potential antitumor activity, with low toxicity and minimal side effects.[26,27] By activating the cellular antioxidant system, zinc shifts redox balance towards a reductive state, slightly

inhibiting cell proliferation. Combining zinc with the ligand Carbidopa may enhance their respective activities.

Very little information regarding the coordination chemistry of carbidopa is available in the literature. Previous reports indicate that carbidopa forms a solid complex with Cr(III), $K_2[Cr(C_2O_4)_2(Carbi)]$. The ligand exhibits the same coordination mode as ZnCarbi and demonstrates antioxidant activity against DPPH and peroxide radicals.[28] A study in solution predicted the most abundant metal complexes with carbidopa at pH 7.4 (L:M 10^{-6}: 10^{-5} mol/L), with divalent ions, as $CuH_{-2}L$, FeL, MnHL, and ZnHL showing dissociation constants, K_d values in nmol/L of $8.11x10^{-6}$, $1.07x10^{4}$, $2.33x10^{2}$, $2.96x10^{6}$.[29] Another study using potentiometric and spectrophotometric methods revealed a 1:2 Fe(II):Carbidopa interaction in solution.[30] Consequently, evaluating the ZnCarbi system and its biological effects is of interest. The complexation of Carbidopa with Zn^{2+} may cause a conformational change in the ligand, enhancing its activity. Our group previously showed that Zn complexes can induce reductive stress in cancer cells.[31] The synthesis and physicochemical characterization of the ZnCarbi complex were performed. To evaluate its biological behavior, we studied the anticancer, mechanistic, and antimetastatic effects of carbidopa and its complex against the triple-negative breast cancer cell line MDA-MB-231. Additionally, we explored their interaction with bovine serum albumin (BSA), a model for human albumin, to determine if the compounds could be reversibly bound, transported, and released by the protein.

Results

The $[Zn(Carbi)(H_2O)_2].2H_2O$ complex (Figure 1) was synthesized by adding a solution of $ZnCl_2$ (1 mmol) in 700 µL of water to carbidopa (0.5 mmol) in 40 mL of methanol. The mixture was stirred under nitrogen for 4 h (pH = 5). The resulting white precipitate was filtered, washed, and dried under nitrogen (see Supporting Information). Based on experimental data, including elemental and thermogravimetric analysis, conductimetry, and additional physicochemical characterization (detailed below), the proposed structure for the complex was determined.

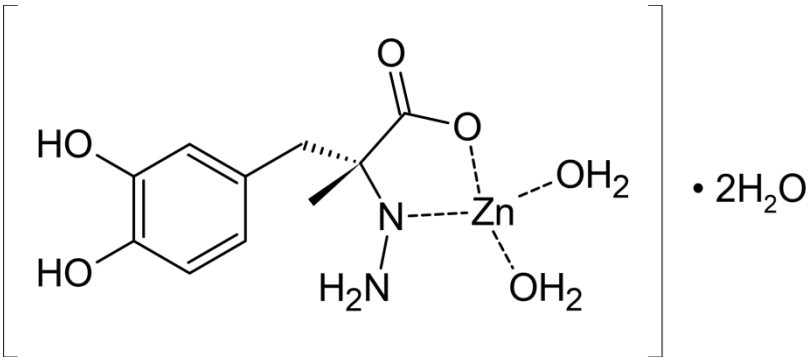

Figure 1 Suggested structure for ZnCarbi

Characterization in solid state. FTIR spectroscopy

The FTIR spectrum of carbidopa exhibits strong and broad bands between 3000 and 2400 cm^{-1}, which are attributed to hydrogen bond formation between COO…H…NH groups (Figure S2). The strong band at 3531 cm^{-1} shifted to 3432 cm^{-1} upon complexation, while the bands associated with intraligand hydrogen bonding disappeared. For the carbidopa-related compound L-dopa, the C=O stretching of the COOH group appeared at 1656 cm^{-1} indicating the presence of a double bond in the C=O group of the carboxylic acid moiety.[32] In carbidopa, however, this band splits into two peaks, at 1604 cm^{-1} and 1405 cm^{-1}, corresponding to the antisymmetric and symmetric stretching vibrations of the carboxylate group. This splitting

suggests the deprotonation of the acid and the formation of a COO^- anion, consistent with its zwitterionic structure.[33,34]
In the case of ZnCarbi, these bands were observed at 1604 and 1394 cm^{-1}, indicating monodentate coordination (Figure S2). The band associated with C-OH bending, which is located at 1242 cm^{-1} in carbidopa, remained at 1236 cm^{-1} after complexation. Additionally, bands corresponding to NH and NH_3^+ bending in carbidopa (1529, 1371 and 1100 cm^{-1}) showed reduced intensities due to deprotonation and interaction with the metal. The N-N stretching mode (1017 cm^{-1}) and the C-N stretching mode (1175 cm^{-1}) appeared with low intensity in ZnCarbi.[35]
Collectively, this spectral data suggests that carbidopa coordinates to Zn(II) ion through the carboxylate and deprotonated NH groups.

Characterization in solution. NMR spectroscopy
The NMR spectrum of ZnCarbi (Figure S3) was compared with the predicted spectrum for carbidopa.[36,37]
A similar predicted ^{1}HNMR spectrum for the ligand was obtained. The chemical shifts of the OH groups (8.67 and 8.86 ppm) indicate the presence of both groups in the ZnCarbi complex, suggesting that these groups remained intact after metal complexation. However, the chemical shifts of the COOH and NH_2 groups could not be determined, possibly due to the zwitterionic structure of carbidopa[34] or the exchange of protons bonded to O and N atoms with the solvent protons. Nevertheless, the NH chemical shift of (C_{chiral})-NH-(NH_2) bond of the ligand (4.24 ppm) disappears upon complexation, indicating interaction with Zn.
The ^{13}CNMR spectra show a difference in the chemical shift of the COO^- group (174.9 ppm for carbidopa and 177.2 ppm ZnCarbi, very weak), indicating potential coordination of the carboxylate anion to the metal center. Additionally, the chemical shift of the chiral C atom (C-N bond) shifted from 65.2 ppm (carbidopa) to 66.3 ppm (ZnCarbi), suggesting that both functional groups interact with the metal center. These results align with the coordination modes observed in the FTIR analysis.
Based on these physicochemical determinations, the proposed structure of the $[Zn(Carbi)(H_2O)_2].2H_2O$ complex is depicted in Figure 1.

Stability determinations
The stability of $[Zn(Carb)(H_2O)_2].2H_2O$ was assessed using UV-vis and conductivity assays at 25 °C. Molar conductivity measurements of a 10^{-3} M solution of ZnCarbi in DMSO and H2O/DMSO mixture (95/5) remained constant over a period of 4 h (12 $\Omega^{-1}cm^2mol^{-1}$), indicating that the complex is stable, at least during the preparatory phase for biological testing. This stability was further supported by electronic spectroscopy, as the UV-vis spectra of ZnCarbi in DMSO and the H2O/DMSO mixture (95/5) showed no change over 4h (Figures S4a and S4b, respectively).
Under the experimental conditions of this study, the complex does not display signs of decomposition within the 15 min prior to cellular inhibition assays. For potential future medicinal applications, complementary studies should be conducted.[38]

Interaction with Bovine serum albumin (BSA)
The major drug carrier protein in human blood plasma is human serum albumin (HSA). Bovine serum albumin has been used as a model for the study of the interaction of different compounds with the protein, instead of HSA, because of its abundance and low cost. The major intrinsic fluorescence of BSA, located at positions 134 and 212, has been assigned to the two tryptophan residues. A decrease in fluorescence was observed when BSA, 6 µM, was titrated with different concentrations of carbidopa and ZnCarbi, indicating the interaction of the compounds with albumin. This quenching of fluorescence emission was measured after an incubation time of 20 min. Due to the intrinsic absorbance of both the ligand and the complex, deconvolution processes were performed on the experimental curves, instead of using the correction by inner filter. The corrected spectra are shown in Figures S5a and S5b.

To analyze the quenching mechanism (static or dynamic) the ratio of fluorescence intensities in the absence (F_0) and the presence of the quencher (F) was plotted against the quencher concentration [Q] (Figure 2). From these plots, K_{SV} (Stern-Volmer quenching constant) and K_q (bimolecular quenching constant) were calculated according to the Stern-Volmer equation: $F_0/F = 1 + K_q\tau_0[Q] = 1 + K_{SV}[Q]$ (Table 1), where τ_0 is the lifetime of the fluorophore in the absence of quencher considered as 1×10^{-8} for a biopolymer. The linearity of these graphs at lower concentrations is indicative of a static quenching for both compounds. Besides, the calculated K_q values resulted greater than the maximum dynamic quenching constant, 2.0×10^{10} $M^{-1}s^{-1}$, indicating a static quenching as the most probable interaction for both compounds.

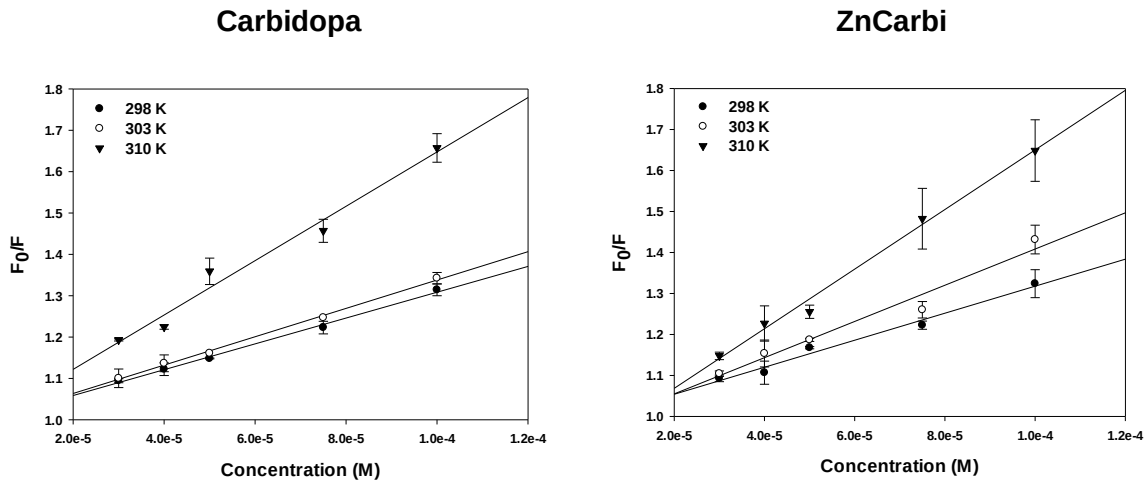

Figure 2 Plots of F_0/F vs [Q] for carbidopa and ZnCarbi at 298, 303 and 310 K. Results represent the mean values ± the standard error of the mean (SEM) from three separate experiments

Table 1. Stern-Volmer constant (K_{sv}), quenching rate constant (K_q), binding constant (K_a) and n binding sites for the interaction of carbidopa and ZnCarbi with BSA (6 µM) in Tris-HCl buffer (0.1 M, pH 7.4).

Carbidopa	Ksv x 10^3 M^{-1}	Kq x 10^{11} $M^{-1}s^{-1}$	log K_a	K_a x 10^3 M^{-1}	n
298 K	3.12 ± 0.13	3.12	3.46 ± 0.20	2.88 ± 0.17	1.00 ± 0.05
303 K	3.44 ± 0.18	3.44	3.61 ± 0.17	4.07 ± 0.19	1.02 ± 0.05
310 K	6.58 ± 0.43	6.58	3.93 ± 0.21	8.51 ± 0.67	1.03 ± 0.06
Zn Carbi					
298 K	3.30 ± 0.16	3.30	3.73 ± 0.19	5.37 ± 0.32	1.06 ± 0.06
303 K	4.42 ± 0.25	4.42	4.04 ± 0.21	10.96 ± 0.90	1.11 ± 0.08
310 K	7.27 ± 0.36	7.27	4.74 ± 0.24	54.95 ± 4.29	1.23 ± 0.08

The modified Stern-Volmer equation (log $[(F_0\text{-}F)/F]$ = log K_a + n log [Q]) allows the determination of the equilibrium between free and bound compounds and the binding constant, K_a, can be determined to understand the distribution of compounds in plasma. In this equation, n is the number of binding sites. Figure 3 shows the graphs log $[(F_0\text{-}F)/F]$ *vs.* log [Q] from which the K_a and n values were calculated (Table 1).

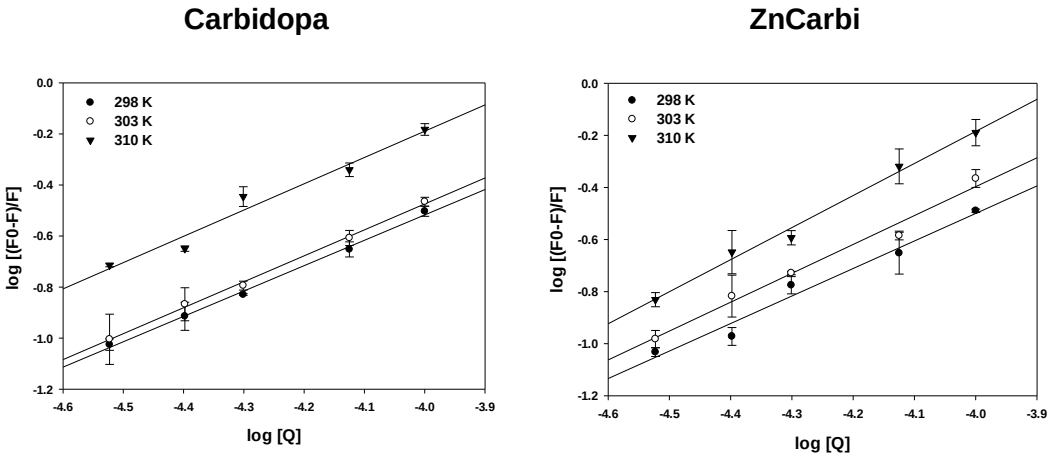

Figure 3 Plot of log [(F_0–F)/F] vs. log [Q] for carbidopa and ZnCarbi systems at T = 298, 303 and 310 K. Results represent the mean values ± the standard deviation (SD) error from three separate experiments

From these values it can be seen that the binding of both compounds increase at higher temperatures. Moreover, ZnCarbi binds BSA stronger than carbidopa. The number of binding sites with high affinity resulted near 1.0 in both cases. Binding constants of *ca.* 1000 M^{-1} indicate a moderate binding to the protein in which the compound could be transported and released from the protein. The binding of the related compound L-dopa with HSA resulted on the same order of magnitude (2.3 x 10^4 M^{-1}, experimental and 3.5 x 10^3 M^{-1}, computationally calculated).[39]
The thermodynamic parameters, free energy change (ΔG), entropy change (ΔS) and enthalpy change (ΔH) help determine the nature of the interaction between each compound and BSA. These parameters can be obtained using the van't Hoff equation: ln K_a = - ΔH/RT+ ΔS/R, where R is the gas constant (8.3145 J x K^{-1} x mol^{-1}). Thermodynamic parameters were obtained from the plots of ln K_a *vs.* 1/T (Figure S6) and are summarized in
Table **2**.

Table 2. Thermodynamic parameters for the interactions between carbidopa and ZnCarbi with BSA.

	T (K)	ln Ka	ΔH^o KJ/mol	ΔS^o KJ/mol.K	ΔG KJ/mol
Carbidopa	298	7.96	60.47 ± 3.36	0.27 ± 0.01	- 19.73 ± 1.19
	303	8.30			- 21.08 ± 1.27
	310	9.05			- 22.96 ± 1.39
ZnCarbi	298	8.58	129.91 ± 6.71	0.51 ± 0.02	- 20.95 ± 1.41
	303	9.30			-23.48 ± 1.58
	310	10.91			- 27.03 ± 1.83

The negative free energy change, estimated using the equation: ΔG = ΔH – TΔS is indicative of a spontaneous process. The signs obtained from these parameters are an indication of the type of forces acting between the protein and the compounds. For carbidopa and ZnCarbi the changes in enthalpy and entropy resulted in positive values. These results agree with hydrophobic association, in which a partial withdrawal of the non-polar group from water exists. That is to say, that as in the case of amino acids, the hydrophobic side chains become buried by complexation with BSA producing an enhancement of the disorder of the unstructured water molecules. At higher temperatures, the solvent structure is less ordered and the positive

contribution to the entropy decreases, being the process enthalpy driven and the free energy and the values of K_a increase.[40]

Anticancer effects

Cell viability assays

Initially, the effects of 100 μM ZnCarbi, incubated for 24 h, were tested across different cell lines (Figure 4). The complex did not exert deleterious effects in human lung adenocarcinoma A549 cells, human colon cancer (HCT116) cells and murine breast cancer LM3 cells. The MDA-MB-231 cell line was chosen for further studies because the metal complex was found to reduce cell viability.

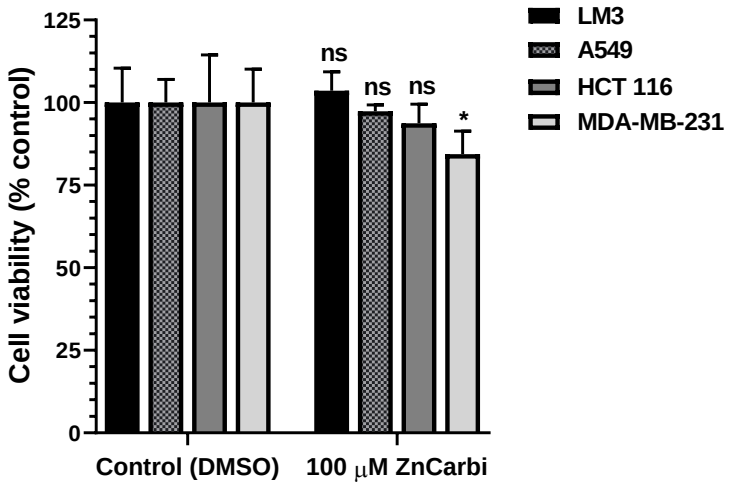

Figure 4 Effects of 100 μM ZnCarbi (24 h incubation) on cell viability. The results are expressed as the percentage of the basal level and represent the mean ± SEM from three separate experiments. * Significant values in comparison with the control level ($P < 0.05$)

As previously mentioned, MDA-MB-231 is a triple-negative cell line that lacks expression of the estrogen receptor, progesterone receptor, or HER2 protein, which limits therapeutic options due to the absence of hormone receptors. The cells exhibit invasiveness *in vitro* and metastasize to lymph nodes *in vivo*. Previous studies have shown that carbidopa can act as an inhibitor of MDA-MB-231 breast cancer cell growth.[8,41]

To evaluate the cytotoxicity of both the ligand and the complex in the MDA-MB-231 breast cancer cell line, the effects of these compounds were evaluated by the MTT assay (Figure 5). Cell viability decreased in a dose-response manner, and complexation with carbidopa enhanced the anticancer properties of the ligand. The half maximal inhibitory concentrations (IC_{50}) were determined as follows: IC_{50} for carbidopa, 206.28 μM and IC_{50} for ZnCarbi, 151.48 μM. To further elucidate the potential cytotoxic pathways, we investigated the effects of the compounds on cell morphology, oxidative-reductive stress (by measuring ROS and GSH/GSSG contents), inhibition of cell death induced by H_2O_2, and disruption of mitochondrial membrane potential.

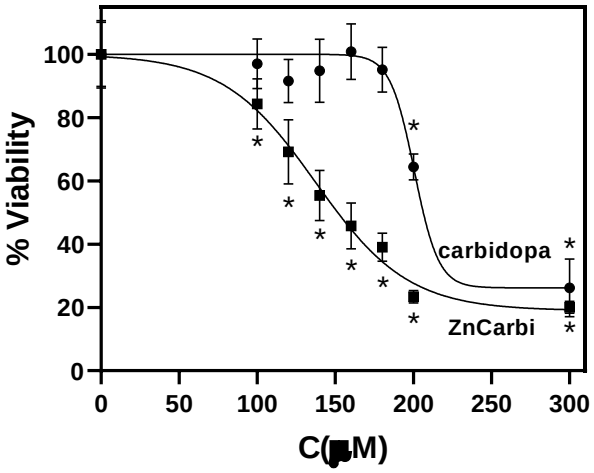

Figure 5 Effects of carbidopa and ZnCarbi (24 h incubation) on cell viability of MDA-MB231 breast cancer cell line. The results are expressed as the percentage of the basal level and represent the mean ± SEM from three separate experiments. * Significant values in comparison with the control level ($P < 0.05$)

The *in vitro* toxicity of carbidopa and ZnCarbi was assessed using the normal HEK293 cell line, derived from human embryonic kidney cells. No deleterious effects were observed at concentrations higher than the IC_{50} values of both compounds (Figure 6), indicating that the compounds exhibit selective action towards the cancer cell line.

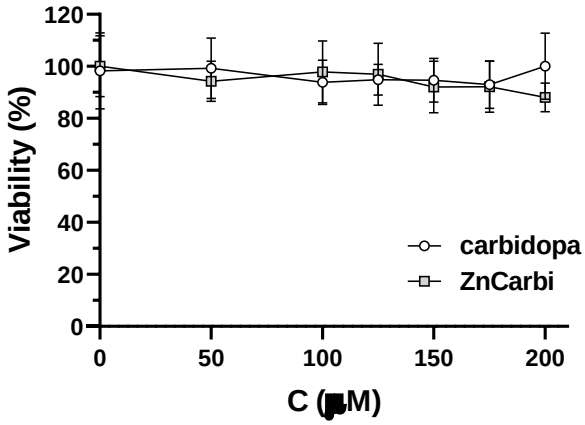

Figure 6 Effects of carbidopa and ZnCarbi (24 h incubation) on cell viability of a non-tumoral HEK293 cell line. The results are expressed as the percentage of the basal level and represent the mean ± SEM from three separate experiments. No significant values in comparison with the control level ($P < 0.05$), up to 200 μM concentrations

Cell Morphology

The morphological effects of the studied compounds on the MDA-MB-231 cell line were evaluated using the crystal violet staining assay. This dye, which has a positive charged structure, can penetrate the cell membrane and bind to anionic proteins and DNA, resulting in cells exhibiting a violet coloration. While this staining technique does not provide detailed ultrastructural information, it allows for the assessment of cell shape, size, and overall structure under the microscope. Additionally, it provides insight into general cellular contents, including the cytoplasm and, in eukaryotic cells, the nucleus.[42]

From the obtained photographs (Figure S7), it is clear that untreated MDA-MB-231 breast cancer cells exhibit their characteristic epithelial morphology and spindle-shaped appearance (long and thin). Compared with control (0.5% DMSO), treatment with 151.5 μM of carbidopa, did not induce any appreciable morphological changes. However, after 24 h of treatment with ZnCarbi at its IC_{50} value (151.5 μM), there was a notable reduction in cellular nuclear volume, presence of pyknotic nuclei, membrane protrusions and a considerable decrease in cell numbers. These observations suggest the activation of programmed cell death processes, such as apoptosis.

Cellular ROS and GSH/GSSG ratio

The antioxidant properties of carbidopa have been documented in neuroblastoma cells,[43] peripheral blood lymphocytes, and through the Trolox antioxidant assay.[44] Carbidopa has been shown to interact with the antioxidant intracellular pathway, leading to the upregulation of antioxidant enzyme expression. We have found similar results when measuring ROS generation in the MDA-MB-231 cell line after 24 h incubation with carbidopa and ZnCarbi. Both compounds led to a decrease in ROS levels, as illustrated in Figure 7a, suggesting that cell death may occur through reductive stress mechanisms. This effect was consistently observed during a 4 h incubation at the higher tested concentrations of the compounds. Furthermore, treatment with both carbidopa and ZnCarbi resulted in a dose-dependent increase in the levels of the natural antioxidant tripeptide glutathione and the oxidized glutathione (GSH/GSSG) ratio after 24 h, as shown in Figure 7b.

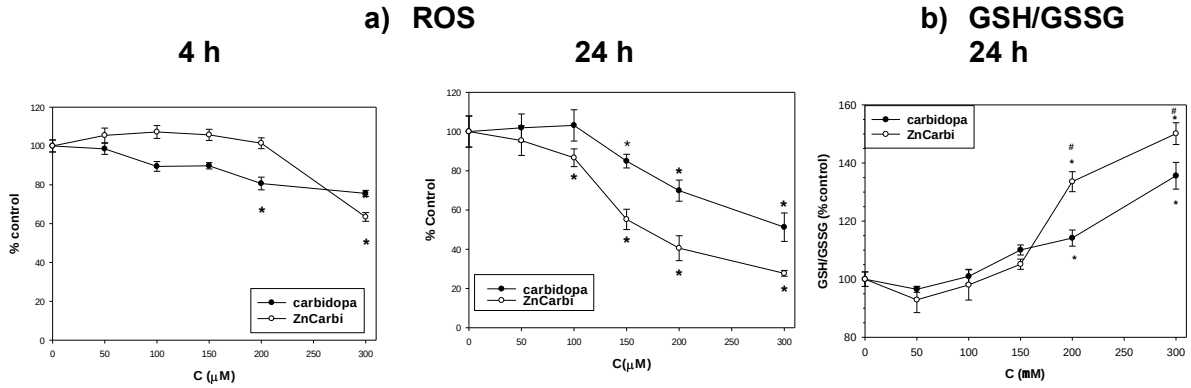

Figure 7 Measurement of reductive stress. Effects of carbidopa and ZnCarbi on **a)** ROS decrease at 4 h and 24 h incubation and **b)** increase in the GSH/GSSG ratio, in MDA-MB-231 cells. The results are expressed as the percentage of the control and represent the mean ± SEM from three separate experiments. * Significant values in comparison with the control level ($P < 0.05$). # Significant difference between ZnCD and CD levels at the same concentration ($P < 0.05$).

Improvement of cell survival in H_2O_2-induced apoptosis

The protective effects of carbidopa against H_2O_2-induced DNA damage have been documented in the human neuroblastoma SH-SY5Y cell line[43] and in healthy human peripheral blood lymphocytes.[44] We subsequently assessed the cellular antioxidant properties of carbidopa and ZnCarbi by the determination of their ability to mitigate cell death caused by hydrogen peroxide (H_2O_2) in the MDA-MB-231 cell line. Protection was evaluated by preincubation with the compounds. As shown in Figure **8**, carbidopa prevented the decrease in cell viability at a concentration of 150 μM, while ZnCarbi exhibited protective effects at 100 μM when exposed to hydrogen peroxide at both 100 and 300 μM concentrations. This behavior is consistent with the higher antioxidant efficacy demonstrated by ZnCarbi (see Figure **8**). These findings suggest that the tested compounds may enhance cell survival in H_2O_2-induced apoptosis in MDA-MB-231 cells, likely due to their reductive stress behavior, effectively scavenging free radicals produced in solution.

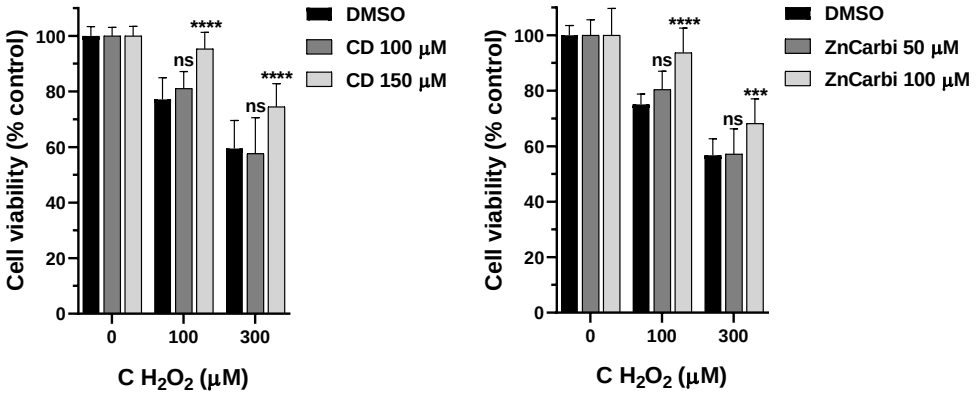

Figure 8 Protective effects of carbidopa and ZnCarbi, at different concentrations, on H_2O_2 (100 and 300 μM) induced apoptosis on MDA-MB-231 cell line. The compounds were incubated during 2 h, then, cells were washed, before the addition of H_2O_2 followed by 24 h incubation. Data are represented as means ± SEM of three independent experiments. *** : $P < 0.001$; **** : $P < 0.0001$: Significant values in comparison with the level of control group pre-incubated for 2 h with 0.5% DMSO

Mitochondrial membrane potential changes

The mitochondrial membrane potential (MMP) in cancer cells typically surpasses that of normal cells, and a reduction in MMP can lead to decreased cell viability in cancer cells.[45] To evaluate the effects of carbidopa and ZnCarbi in MMP, MDA-MB-231 cells were treated with the compounds during 24 h, and then exposed to the $DIOC_6$ probe. This green fluorescent, lipophilic dye selectively targets the mitochondria of live cells. As shown in Figure 9, both carbidopa and ZnCarbi induce mitochondrial depolarization. The reductive stress, measured by the increase in the GSH/GSSG ratio, creates an imbalance in the cellular redox state. This condition affects the mitochondrial function, particularly through its impact on the MMP. Excess reducing equivalents can overcharge the mitochondrial electron transport chain due to the reduction of the redox sensitive proteins, leading to a "backlog" of electrons that impair its efficiency. This state enhances the potential for electron escape, resulting in a reverse electron transport and ROS production, even in a reducing environment. The paradoxical rise in ROS damages mitochondrial lipids, proteins, and DNA, ultimately leading to MMP depolarization. The disruption on ATP production activates downstream stress responses, including the opening of the mitochondrial permeability transition pore. Besides, excess of GSH disturbs the thioredoxin (Trx) and glutaredoxin (Grx) homeostasis, components of the mitochondria that play an important role in DNA synthesis, governing protein folding, and regulation of cell growth/apoptosis. Those processes can trigger cell death pathways. Chronic reductive stress also alters signaling pathways and transcription factors, such as NF-κB, further exacerbating mitochondrial dysfunction and cellular damage. [46-49]

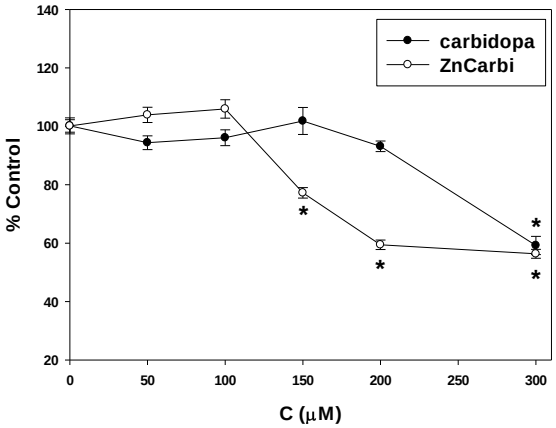

Figure 9 Effects of the addition of increasing concentrations of carbidopa and ZnCarbi during 24 h, on the changes of the mitochondrial membrane potential in MDA-MB-231 cells. Each point represents the mean ± SEM of three measurements in three independent experiments. Significant differences: * $P < 0.05$ compared to the control

Antimetastatic studies

Wound healing assay

Cell migration plays a crucial role in cancer metastasis. To simulate *in vivo* cell migration during wound healing, we applied a standard *in vitro* technique for the measuring migration in two dimensions. Figure S8 presents images from the scratch wound healing assay for the control, carbidopa, and ZnCarbi. MDA-MB-231 breast cancer cells were wounded with a pipette tip and treated with 50 μM of either carbidopa or ZnCarbi. Microscopic observations were recorded at the initial scratch (t = 0) and after 24 h of incubation with the compounds.

As shown in Figure 10, both carbidopa and ZnCarbi inhibited cancer cell migration compared to the untreated condition. Notably, ZnCarbi showed a greater inhibition of cell migration than carbidopa. In contrast, another study using the wound healing assay found that treatment with 15 μM of carbidopa did not significantly affect the migration of the triple negative MDA-MB-231 cancer cell line.[8]

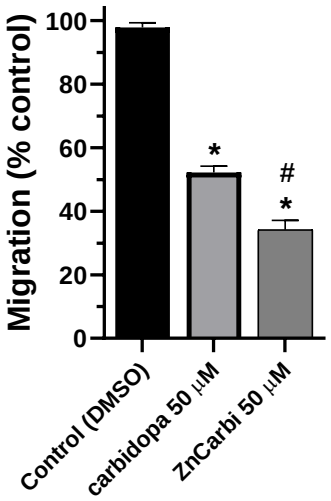

Figure 10 Cell migration (scratch wound healing assay) using a monolayer of breast cancer cell line MDA-MB-231. Values of percentage migration ± SEM for three independent measurements. * $P < 0.05$ with respect to the control and # $P < 0.05$, between carbidopa and ZnCarbi

Transwell migration assay

The wound healing assay measures random cell migration since it does not create chemotactic gradient. In contrast, the Transwell migration assay allows for the study of directional migration by establishing a chemotactic gradient using a chemoattractant. In this test, cells migrated through the 8 µm porous membrane from the upper chamber to the lower chamber, driven by the gradient created by the culture media containing 10% (v/v) FBS in the lower chamber. Under the same conditions as the wound healing assay, treatment with 50 µM carbidopa and ZnCarbi, significantly reduced the number of migrating MDA-MB231 cells by 57 % and 71 %, respectively (**Figure 11** and S9). This method confirms the inhibitory effect of carbidopa on MDA-MB-231 cell migration, particularly at a 50 µM concentration.

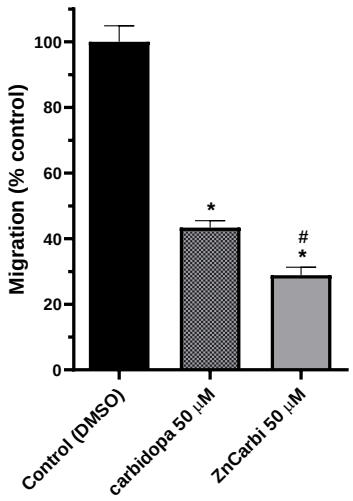

Figure 11 Analysis of breast cancer cell migration assessed by *in vitro* Transwell assay. Percentage of migrated cells after 24 h of treatment of carbidopa, ZnCarbi and 0.5% DMSO (control), with 10% FBS as chemoattractant. Cells were counted from 20 random microscope fields for each sample. Values are represented as the mean percentage of migration (relative to control) ± SEM for three independent measurements. * $P < 0.05$ compared to the control and # $P < 0.05$, between carbidopa and ZnCarbi

Invasion Transwell assay

The Transwell invasion experiment follows a similar procedure to the Transwell migration assay, with the key difference being the addition of a thin layer of extracellular matrix (ECM, Matrigel) on the porous filter before seeding the cells into the upper chamber. The EMC blocks the membrane pores, preventing the migration of non-invasive cells. On the other hand, invasive cells have the ability to degrade the matrix, pass through the ECM layer, and adhere to the bottom of the filter. As shown in Figure 12 and S10, treatment with 50 µM of the ZnCarbi complex resulted in a 40% reduction in cell invasion. Carbidopa, in contrast, did not show significant differences compared to the untreated cells.

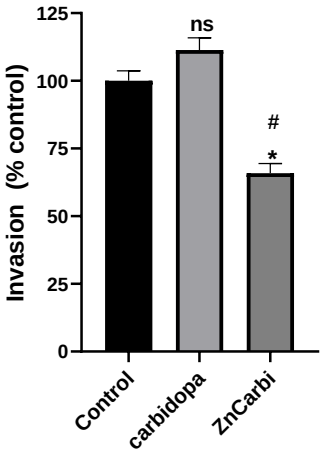

Figure 12 Analysis of breast cancer cell invasion assessed by *in vitro* Transwell assay. MDA-MB-231 cell counts were recorded after 24 h of treatment with 50 µM carbidopa and ZnCarbi and 0.5% DMSO (control) from 20 random microscope fields for each sample. Values are represented as the mean cell count (percentage relative to control) ± SEM for three independent measurements. * $P < 0.05$ compared to the control and # $P < 0.05$, between carbidopa and ZnCarbi

Discussion

A delicate balance between oxidants and antioxidants is crucial for maintaining cellular redox homeostasis and metabolism, thereby preventing oxidative or reductive damage. Normal cells typically bear lower levels of ROS and antioxidants compared to cancer cells. ROS homeostasis plays a vital role in keeping cells viable and functional among fluctuations in oxidant or antioxidant systems. Conversely, tumor cells with elevated levels of ROS in comparison with normal cells due to an imbalance between oxidants and antioxidants tend to be more susceptible to a substantial increase in ROS, resulting in decreased cell viability. However, excessive antioxidant agents can disrupt mitochondrial homeostasis, and be detrimental to cells. Hence, substances that induce stress, whether oxidative or reductive, can effectively cause cell death in cancer cells.[50–52]

Reductive stress occurs when there is an excess of reductants enhancing antioxidant mechanisms. However, like oxidative stress, reductive stress can be detrimental and may evolve mitochondrial dysfunction and cytotoxicity.[48] Reductive stress has been associated with various biological dysfunctions, including cardiovascular diseases and diabetes in mice.[53] Metal complexes of Zn with sartans have demonstrated anticancer activity, enhancing the effects of the ligands. Depending on the ligand, cellular ROS production (as seen with telmisartan[54], azilsartan[55], losartan[56]) or depletion (as with candesartan and valsartan) influenced the improved anticancer effects of the complexes in human lung A549 cancer cell lines, which maintained oxidative or reductive stress for their cytotoxic behavior.[31] Zn(II) ion resulted non-toxic in those cancer cells but affect cellular ROS production. It has also been reported that carbidopa causes cellular ROS depletion and an increase in the GSH/GSSG

ratio. In this study, we show that Zn coordination improved both the antioxidant action and cytotoxic effect of carbidopa in a cancer cell line by modifying its structure.

Other ligands, such as flavonoids, maintain or increase the cellular ROS levels in cancer cells after 24 h incubation Their complexes with other elements, like vanadium, further enhance ROS production.[57] It is important to note that in *in vitro* experiments, both ligands and their complexes acted as antioxidants, with this effect being more pronounced in metal complexes due to increased resonance in the aromatic rings of flavonoids in their radical form, caused by the electron-withdrawing properties of the metal ions. For example, Zn/rutin showed significantly greater superoxide and DPPH radical scavenging activity compared to rutin alone. Additionally, the complex enhanced the cytotoxic activity of the ligand against the acute myeloid leukemia cell line (KG1) and the RPMI8226 multiple myeloma cell line, with IC_{50} values of 91.4 µM and 196.6 µM, respectively, after 24 h incubation.[58] These IC_{50} values are similar to those observed for the VO/rutin complex (IC_{50}, 98 µM in human lung A549 cancer cell line), which induces cellular oxidative stress, while the ligand alone did not affect ROS generation up to 100 µM concentration. The Zn/morin complex also exhibited anticancer activity against A549 and H520 cancer cell lines with values of IC_{50} around 50 µM, similar to those of VO/morin complex in T47D and SKBR3 breast cancer cells, where the latter complex showed increased ROS production. The Cu/morin complex improved the anticancer activity of morin in the human laryngeal epidermoid Hep-2 and baby hamster kidney BHK-21 cell lines. *In vitro* antioxidant assays against the DPPH radical also demonstrated higher antioxidant activity for the morin complexes with Zn^{2+}, VO^{2+}, Cr^{2+}, and Cu^{2+} compared to the free ligand.[59]

Reports of Zn/chrysin complex indicate a higher radical scavenging activity compared to the free ligand, while a similar antioxidant activity was observed for the Zn/quercetin complex compared to quercetin alone.[60] Enhanced antioxidant effects were also noted for $V^{IV}O$ complexes of chrysin and quercetin.[57] Zn/quercetin demonstrated increased cytotoxicity against A549 human lung cancer cells, as well as human hepatocarcinoma cell lines HepG2, SMMC-7721,[61] and bladder cancer BFTC-905 cells, compared to quercetin, primarily through the induction of apoptosis and intercalation into DNA. Notably, Zn resulted non-toxic to the cells.[62] The $V^{IV}O$ complex, VO/quercetin generated ROS in A549 cancer cells, leading to a decrease in cell viability (unpublished data). Measurements of the behavior of $V^{IV}O$ in A549 cell lines up to 100 µM, indicated that the metal had no impact on ROS production and little effect on cellular cytotoxicity.[57] Although flavonoids up to 100 µM do not generate ROS in the tested cancer cells, their interaction with a metal with redox properties leads to cellular ROS production, acting as pro-oxidant agents. However, in *in vitro* assays, vanadium complexes generally enhance the antioxidant capacity of flavonoids (antioxidant agents). For oxidovanadium(IV) complexes with the natural polyphenols, flavonoids, an oxidative stress-induced apoptotic cancer cell death mechanism was observed.[57] For the Zn/flavonoid complexes mentioned, there is no reported data on cellular ROS production or depletion. However, with sartans and carbidopa, the complexes involving the redox-inactive Zn(II) metal ion, retain the redox properties of the ligands in cancer cells, and improved their anticancer effects, probably due to the rigidity conferred to the ligand upon metal coordination.

Both compounds enhanced cell survival in H_2O_2-induced apoptosis due to their antioxidant properties, with the ZnCarbi complex showing stronger protection at lower concentrations. Cancer metastasis involves several steps, with invasion and migration being key. [63] ZnCarbi significantly reduced migration and invasion in MDA-MB-231 cancer cells, even at non-cytotoxic concentrations, indicating these effects were not due to cytotoxicity. Protein binding studies with BSA revealed strong binding affinity (10^3 to 10^4 M^{-1}), showing static quenching and hydrophobic interactions, with a single binding site for the complex on the BSA molecule.

Conclusions

In summary, this study showed that complexing carbidopa with zinc enhances its anticancer efficacy against the MDA-MB-231 triple-negative breast cancer cell line. The ZnCarbi complex improved reductive status and protected against H_2O_2-induced damage, suggesting that metal complexation improves the ligand's cytotoxicity. Morphological changes and mitochondrial membrane disruption point to apoptosis as a key mechanism. Additionally, ZnCarbi reduced

cell invasion and migration, indicating potential to prevent metastasis at non-toxic concentrations. Binding studies suggest that the compounds can be effectively transported by albumin.

Supporting Information

Experimental. Materials and Methods. Preparative $[Zn(Carb)(H_2O)_2].2H_2O$ complex. In vitro bovine serum albumin (BSA) interaction. Cell culture assays. Antimetastasic studies. Analytical Statistics. **Figure S1**. Thermogravimetric curve for ZnCarbi. Oxygen flow of 50 mL min^{-1}; heating rate 10 °C min^{-1}. The inset shows amplification of the weight loss up to 225 ºC. **Figure S2** FTIR spectra of carbidopa and ZnCarbi. **Figure S3.** a) experimental ^{1}H and ^{13}C RMN spectra of ZnCarbi. b) Predicted ^{1}H and ^{13}C RMN spectra of carbidopa. **Figure S4.** Variation of the electronic spectra of ZnCarbi with time. a) DMSO, 7 x 10^{-4} M; b) H_2O/DMSO (95/5), 1 x 10^{-4} M. **Figure S5. S5a** Quenching of fluorescence of BSA by carbidopa obtained after deconvolution. Concentrations of carbidopa and BSA: 0-100 µM and 6 µM, respectively. T = 298, 303 and 310 K. **S5b** Quenching of fluorescence of BSA by ZnCarbi obtained after deconvolution. Concentrations of ZnCarbi and BSA: 0-100 µM and 6 µM, respectively. T = 298, 303 and 310 K. **Figure S6** Plots of ln K_a vs. 1/T for carbidopa and ZnCarbi. T = 298, 303 and 310 K. **Figure S7** Cellular morphology of the MDA-MB-231 breast cancer cell line incubated with 151.5 µM solutions of carbidopa and ZnCarbi, 24 h, 40X. **Figure S8** Wound healing assay to determine cell migration. Wound-healing assays were performed 50 µM carbidopa and ZnCarbi treated cells and untreated cells used as controls. Representative phase-contrast microscope images showing the area covered by the cells. Original magnification 10X. **Figure S9** Photographs of cell migration through the polycarbonate membrane stained by crystal violet. **Figure S10** Photographs of cell invasion through the Matrigel-coated polycarbonate membrane stained with crystal violet. The authors have added Figure S1 and cited additional references within the Supporting Information.[64,65]

Acknowledgments

This work was supported by CICPBA, ANPCyT, CONICET and UNLP, Argentina. LGN, VM and EGF are members of the Research Career, CONICET,Argentina. PAMW is member of the Research Career, CICPBA. AAD is fellowship holder from CONICET. This research was funded by the Agencia Nacional de Promoción Científica y Tecnológica (ANPCyT, PICT 2019-0945) and Universidad Nacional de La Plata (UNLP X871 and X1031).

Competing Interests

The authors declare no conflicts of interest.

Author contributions

Conceptualization, P.A.M.W.; validation, E.G.F., L.G.N. and P.A.M.W.; formal analysis, A.A.D. and L.G.N.; investigation, A.A.D., and V.M.; resources, P.A.M.W.; writing-original draft preparation, L.G.N. and P.A.M.W.; writing-review and editing, E.G.F., L.G.N. and P.A.M.W..; visualization, P.A.M.W.; supervision, P.A.M.W. and L.G.N.; project administration, P.A.M.W.; funding acquisition, P.A.M.W. All authors have read and agreed to the published version of the manuscript.

Data availability

The data that support the findings of this study are available from the corresponding author upon reasonable request.

References

[1] World Health Organization, "Breast Cancer", can be found under https://www.who.int/news-room/fact-sheets/detail/breast-cancer, **2024** (accessed 10 September 2024)

[2] P. Giovannelli, M. Di Donato, F. Auricchio, G. Castoria, A. Migliaccio, *Sci. Rep.* **2019**, *9*, 4490. https://doi.org/10.1038/s41598-019-41016-4

[3] S. Popovic, L. Matovina-Brko, M. Popovic, K. Punie, A. Cvetanovic, M. Lambertini, *Oncol. Res.* **2023**, *31*, 221. https://doi.org/10.32604/or.2023.028525

[4] C.D. Marsden, P.E. Barry, J.D. Parkes, K.J. Zilkha, *J. Neurol. Neurosurg. Psychiatry* **1973**, *36*, 10. https://doi.org/10.1136/jnnp.36.1.10

[5] J, Ogura, S, Miyauchi, K, Shimono, S, Yang, S. Gonchigar, V. Ganapathy, Y.D. Bhutia, *Biochem. J.* **2017**, *474*, 3391. https://doi.org/10.1042/BCJ20170583

[6] Z. Chen, A. Cai, H. Zheng, H. Huang, R. Sun, X. Cui, W. Ye, Q. Yao, R. Chen, L. Kou, *Oncogenesis* **2020**, *9*, 49. https://doi.org/10.1038/s41389-020-0236-x

[7] K. Korac, D. Rajasekaran, T. Sniegowski, B.K. Schniers, A.F. Ibrahim, Y.D. Bhutia, *Biochem. J.* **2022**, *479*, 1807. https://doi.org/10.1042/BCJ20210851

[8] Z. Chen, X. Xia, H. Chen, H. Huang, X. An, M. Sun, Q. Yao, K. Kim, H. Zhang, M. Chu, R. Chen, Y.D. Bhutia, V. Ganapathy, L. Kou, *Invest. New Drugs* **2022**, *40*, 1216. https://doi.org/10.1007/s10637-022-01289-5

[9] J.A. Gilbert, L.M. Frederick, M.M. Ames, *Clin. Cancer Res.* **2000**, *6*, 4365.

[10] H. Hanieh, M. Bani Ismail, M.A. Alfwuaires, H.-I.M. Ibrahim, M. Farhan, *Molecules* **2023**, *28*, 3978. https://doi.org/10.3390/molecules28103978

[11] S.R. Lee, *Oxid. Med. Cell. Longev*. **2018**, 9156285. https://doi.org/10.1155/2018/9156285

[12] A.S. Prasad, B. Bao, *Antioxidants* **2019**, 8, 164. https://doi.org/10.3390/antiox8060164

[13] V. Medici, A. Santon, G. Sturniolo, R. D'Incà, S. Giannetto, V. Albergoni, P. Irato, *Arch. Toxicol.* **2002**, 76, 509. https://doi.org/10.1007/s00204-002-0377-z

[14] S.D. Boyd, M.S. Ullrich, J.S. Calvo, F. Behnia, G. Meloni, D.D. Winkler, *Molecules* **2020**, 25, 1086. https://doi.org/10.3390/molecules25051086

[15] M.S. Li, S.E. Adesina, C.L. Ellis, J.L. Gooch, R.S. Hoover, C.R. Williams, *Am. J. Physiol.-Cell Physiol*. **2017**, 312, C47. https://doi.org/10.1152/ajpcell.00208.2016

[16] S.-X. Tan, M. Teo, Y.T. Lam, I.W. Dawes, G.G. Perrone, *Mol. Biol. Cell* **2009**, 20, 1493. https://doi.org/10.1091/mbc.e08-07-0697

[17] D. Cheng, H. Li, S. Hu, T. Zhao, *New J. Chem*. **2022**, 46, 7748. https://doi.org/10.1039/D2NJ00515H

[18] P. Vahidi Ferdowsi, R. Ng, J. Adulcikas, S.S. Sohal, S. Myers, *Molecules* **2020**, 25, 5098. https://doi.org/10.3390/molecules25215098

[19] H. Kumar, R.M. Kumar, D. Bhattacharjee, P. Somanna, V. Jain, *Front. Pharmacol.* **2022**, 13, 720076. https://doi.org/10.3389/fphar.2022.720076

[20] B. Li, W. Cui, Y. Tan, P. Luo, Q. Chen, C. Zhang, W. Qu, L. Miao, L. Cai, *J. Cell. Mol. Med.* **2014**, 18, 895. https://doi.org/10.1111/jcmm.12239

[21] A. Krężel, W. Bal, *Bioinorg. Chem. Appl*. **2004**, 2, 293. https://doi.org/10.1155/S1565363304000172

[22] Y. Xu, A. Li, X. Li, X. Deng, X. Gao, *Biol. Trace Elem. Res.* **2023**, *201*, 739. https://doi.org/10.1007/s12011-022-03166-x

[23] S.A. Lekki-Porębski, M. Rakowski, A. Grzelak, *Biochim. Biophys. Acta BBA - Gen. Subj*. **2023**, 1867, 130447. https://doi.org/10.1016/j.bbagen.2023.130447

[24] K. Jurowski, B. Szewczyk, G. Nowak, W. Piekoszewski, *JBIC J. Biol. Inorg. Chem.* **2014**, 19, 1069. https://doi.org/10.1007/s00775-014-1139-0
[25] R. Sugimoto, L. Lee, Y. Tanaka, Y. Morita, M. Hijioka, T. Hisano, M. Furukawa, *Biol. Trace Elem. Res.* **2024**, *202*, 1937. https://doi.org/10.1007/s12011-023-03818-6
[26] C.Y. Gao, X. Qiao, Z.Y. Ma, Z.G. Wang, J. Lu, J.L. Tian, J.Y. Xu, S.P. Yan, *Dalton Trans.* **2012**, *41*, 12220. https://doi.org/10.1039/c2dt31306e
[27] J. Tan, B. Wang, L. Zhu, *Bioorg. Med. Chem.* **2009**, *17*, 614. https://doi.org/10.1016/j.bmc.2008.11.063
[28] S.S. Rout, S. Pattanaik, S.C. Si, P. Mohanty, *Int. J. Pharm. Pharm. Sci*. **2018**, 10, 137. https://doi.org/10.22159/ijpps.2018v10i1.22464
[29] M. Tosato, V. Di Marco, *Biomolecules* **2019**, 9, 269. https://doi.org/10.3390/biom9070269
[30] T. Fiaz, N. Fatima, S.Z.A. Zaidi, *Pak. J. Chem.* **2013**, 3, 75. https://doi.org/10.15228/2013.v03.i02.p06
[31] V.R. Martínez, M.V. Aguirre, J.S. Todaro, E.G. Ferrer, P.A.M. Williams, *New J. Chem.* **2021**, 45, 939. https://doi.org/10.1039/D0NJ02937H
[32] B. Edwin, J.I. Hubert, *J. Mol. Struct.* **2013**, *1034*, 119. https://doi.org/10.1016/j.molstruc.2012.09.004
[33] B.Z. Chowdhry, T.J. Dines, S. Jabeen, R. Withnall, *J. Phys. Chem. A* **2008**, *112*, 10333. https://doi.org/10.1021/jp8037945
[34] G.M. Sukker, N. Wazzan, R. Hilal, *Indian J. Chem.-A* **2015**, *54A*, 1378.
[35] N.F. Frazão, E.L. Albuquerque, U.L. Fulco, P.W. Mauriz, D.L. Azevedo, *Indian Ocean Rev. Sci. Technol.* **2013**, *3*, 1–12.
[36] À. Pericas, A. Shafir, A. Vallribera, *Org. Lett.* **2013**, *15*, 1448. https://doi.org/10.1021/ol400136y
[37] Z. Talebpour, S. Haghgoo, M. Shamsipur, *Anal. Chim. Acta* **2004**, *506*, 97. https://doi.org/10.1016/j.aca.2003.10.081
[38] G. Ioele, M. Chieffallo, M.A. Occhiuzzi, M. De Luca, A. Garofalo, G. Ragno, F. Grande, *Molecules* **2022**, 27, 5436. https://doi.org/10.3390/molecules27175436
[39] D.P. Yeggoni, R. Subramanyam, *Mol. BioSyst.* **2014**, *10*, 3101. https://doi.org/10.1039/C4MB00408F
[40] P.D. Ross, S. Subramanian, *Biochemistry* **1981**, *20*, 3096. https://doi.org/10.1021/bi00514a017
[41] S. Safe, L. Zhang, *Cancers* 2022, 14, 5574. https://doi.org/10.3390/cancers14225574
[42] M. Feoktistova, P. Geserick, M. Leverkus, *Cold Spring Harb. Protoc.* **2016**. https://doi.org/10.1101/pdb.prot087379
[43] M. Colamartino, L .Padua, C. Meneghini, S. Leone, T. Cornetta, A. Testa, R. Cozzi, *DNA Cell Biol.* **2012**, *31*, 1572. https://doi.org/10.1089/dna.2011.1546
[44] M. Colamartino, M. Santoro, G. Duranti, S. Sabatini, R. Ceci, A. Testa, L. Padua, R. Cozzi, *Neurotox. Res.* **2015**, *27*, 106. https://doi.org/10.1007/s12640-014-9495-7
[45] H,M, Begum, K. Shen, *WIREs Mech. Dis.* **2023**, *15*, 1595. https://doi.org/10.1002/wsbm.1595
[46] P. Fuchs, F. Bohle, S. Lichtenauer, J.M. Ugalde, E. Feitosa Araujo, B. Mansuroglu, C. Ruberti, S. Wagner, S.J. Müller-Schüssele, A.J. Meyer, M. Schwarzländer, *The Plant Cell*, **2022,** *34*, 1375. https://doi.org/10.1093/plcell/koac017
[47] I. Pérez-Torres, V. Guarner-Lans, M.E. Rubio-Ruiz, *Int. J. Mol. Sci.* **2017**, *18*, 2098. https://doi.org/10.3390/ijms18102098

[48] W.X. Ma, C.Y. Li, R. Tao, X.P. Wang, L.J. Yan, *Oxid. Med. Cell Longev.* **2020**, *2020,* 5136957. doi: 10.1155/2020/5136957.
[49] G.A. Kurian, R. Rajagopal, S. Vedantham, M. Rajesh, *Oxid. Med. Cell. Longev.* **2016,** *2016,*1656450. doi: 10.1155/2016/1656450.
[50] A. Krakowiak, S. Pietrasik, *Biology* **2023**, *12*, 875. https://doi.org/10.3390/biology12060875
[51] R. Masella, R. Di Benedetto, R. Varì, C. Filesi, C. Giovannini, *J. Nutr. Biochem.* **2005**, *16*, 577. https://doi.org/10.1016/j.jnutbio.2005.05.013
[52] O. Zitka, S. Skalickova, J. Gumulec, M. Masarik, V. Adam, J. Hubalek, L. Trnkova, J. Kruseova, T. Eckschlager, R. Kizek, *Oncol. Lett.* **2012**, *4*, 1247. https://doi.org/10.3892/ol.2012.931
[53] W. Xiao, J. Loscalzo, *Antioxid. Redox Signal.* **2020**, *32*, 1330. https://doi.org/10.1089/ars.2019.7803
[54] V.R. Martínez, M.V. Aguirre, J.S. Todaro, E.G. Ferrer, P.A.M. Williams, *Biol. Trace Elem. Res.* **2020**, 197, 454. https://doi.org/10.1007/s12011-019-02013-w
[55] V.R. Martínez, M.V. Aguirre, J.S. Todaro, O.E. Piro, G.A. Echeverría, E.G. Ferrer, P.A.M. Williams, *Toxicol. In Vitro* **2018**, 48, 205. https://doi.org/10.1016/j.tiv.2018.01.009
[56] V.R. Martínez, M.V. Aguirre, J.S. Todaro, O.E. Piro, G.A. Echeverría, L.G. Naso, E.G. Ferrer, P.A.M. Williams, *Biol. Trace Elem. Res.* **2018**, 186, 413. https://doi.org/10.1007/s12011-018-1334-x
[57] L.G. Naso, E.G. Ferrer, P.A.M. Williams, *Coord. Chem. Rev.* **2023**, 492, 215271. https://doi.org/10.1016/j.ccr.2023.215271
[58] N.E.A. Ikeda, E.M. Novak, D.A. Maria, A.S. Velosa, R.M.S. Pereira, *Chem. Biol. Interact*. **2015**, 239, 184. https://doi.org/10.1016/j.cbi.2015.06.011
[59] E. Halevas, B. Mavroidi, M. Kaplanis, A.G. Hatzidimitriou, A. Moschona, G. Litsardakis, M. Pelecanou, *J. Inorg. Biochem*. **2022**, 232, 111832. https://doi.org/10.1016/j.jinorgbio.2022.111832
[60] E. Halevas, B. Mavroidi, M. Pelecanou, A.G. Hatzidimitriou, *Inorganica Chim. Acta* **2021**, 523, 120407. https://doi.org/10.1016/j.ica.2021.120407
[61] J. Tan, B. Wang, L. Zhu, *Bioorg. Med. Chem*. **2009**, 17, 614. https://doi.org/10.1016/j.bmc.2008.11.063
[62] Y.-H. Lee, P.-T. Tuyet, *Vitro Cell. Dev. Biol. - Anim.* **2019**, 55, 395. https://doi.org/10.1007/s11626-019-00363-2
[63] T. Efferth, *Int. J. Oncol.* 2009, 34. https://doi.org/10.3892/ijo_00000214
[64] C.E. Säbel, J.M. Neureuther, S. Siemann, *Anal. Biochem.* **2010**, *397*, 218. https://doi.org/10.1016/j.ab.2009.10.037
[65] M.M. Bradford *Anal. Biochem.* **1976**, *72*, 248. https://doi.org/10.1016/0003-2697(76)90527-3

10.1002/cplu.202400596

Table of contents graphic

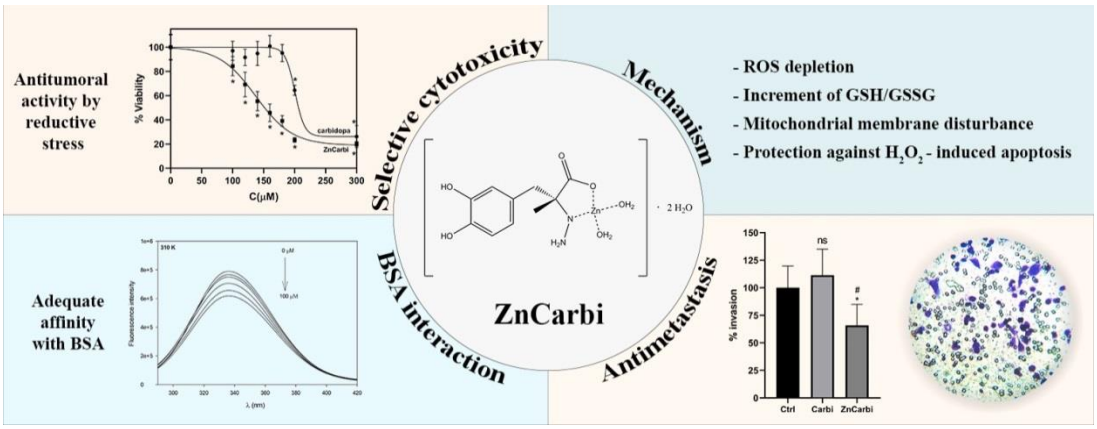

Zn complexation enhances the anticancer effects of carbidopa (ZnCarbi). The complex displayed higher cytotoxicity in MDA-MB-231 triple-negative breast cancer cells. ZnCarbi induces reductive stress, mitigating H_2O_2-induced cell death. The compounds exhibit antimetastatic effects by inhibiting cell migration and invasion and show favorable binding to the carrier protein, bovine serum albumin.